Rolling of a cylinder with slip-dependent friction: The Carter solution revisited

Journal Pre-proof

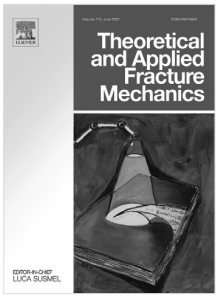

Rolling of a cylinder with slip-dependent friction: The Carter solution revisited

Michele Ciavarella, Luigi Romano, J.R. Barber

PII: S0167-8442(22)00214-2
DOI: https://doi.org/10.1016/j.tafmec.2022.103468
Reference: TAFMEC 103468

To appear in: *Theoretical and Applied Fracture Mechanics*

Received date : 8 March 2022
Revised date : 22 June 2022
Accepted date : 25 June 2022

Please cite this article as: M. Ciavarella, L. Romano and J.R. Barber, Rolling of a cylinder with slip-dependent friction: The Carter solution revisited, *Theoretical and Applied Fracture Mechanics* (2022), doi: https://doi.org/10.1016/j.tafmec.2022.103468.

Rolling of a cylinder with slip-dependent friction: the Carter solution revisited

Michele Ciavarella(1,2), Luigi Romano (3), J.R. Barber (4)

(1) Politecnico di BARI. DMMM department. Viale Gentile 182, 70126 Bari. Mciava@poliba.it, (2) Hamburg University of Technology, Department of Mechanical Engineering, Am Schwarzenberg-Campus 1, 21073 Hamburg, Germany (3) Department of Mechanics and Maritime Sciences, Chalmers University of Technology, Hörsalsvägen 7A, 412 96, Gothenburg, Sweden. luigi.romano@chalmers.se
(4) Department of Mechanical Engineering, University of Michigan, 2350 Hayward Street, Ann Arbor MI 48109-2125, jbarber@umich.edu

Abstract

The problem of a wheel under tractive rolling of Carter is revisited here by assuming a slip-dependent friction force. By assuming a change from static to dynamic friction coefficient occurs over a small distance, we develop effectively a fracture mechanics solution for the shear tractions, which describes some aspects of "falling friction" creepage forces which are commonly observed experimentally. Possible agreement with experiments is discussed, suggesting that friction may include also rate-dependent effects. A simple strip theory is used to estimate 3D effects, which reduce the strength of the singularity at the edges being the peak pressure lower there.

Keywords:
Rolling, Carter solution, Contact Mechanics, Friction model

1. Introduction

In nearly 100 years after the celebrated Carter paper of 1926 [1] which gives the basic solution for an elastic cylinder rolling on an elastic halfspace in the presence of friction, assuming essentially Coulomb friction, we have seen a tremendous development of understanding of the importance of contact mechanics in noise, squeal, wear, corrugation, ride quality, derailments,

etc. Vehicle Dynamic Simulation is today a well established tool for vehicle designers and track engineers for investigating problems which require as ingredient the rapid solution of the frictional rolling contact problem. Kalker [2] has developed many 3D algorithms to permit fast numerical simulation of the behavior of rail vehicles including the basic model for the wheel–rail contact forces. However, while much progress has been obtained not much attention has been paid to the fact that friction is hardly of the Coulomb type, despite there is strong evidence that creepage force does not monotonically grow and saturate as expected from Carter's solution (and indeed any solution assuming Coulomb law), but sometimes shows a maximum and then decays [3,4]. Accurate modelling of creepage curves is important to develop control strategies [5], and "falling friction" is also an important possible explanation of squeal [6,7].

Rabinowicz [8] showed already in the 1950's with simple but elegant experiments on metals, that there is a static friction coefficient f_u, which decays with slip-displacement u to a kinetic value f_d — i.e.

$$f\left(0\right) = f_s \quad \text{and } f\left(u\right) \to f_d\,; \quad u \to \infty\,. \tag{1}$$

We also define the length scale

$$\Delta = \frac{1}{\left(f_s - f_d\right)} \int_0^\infty \left(f(u) - f_d\right) du\,, \tag{2}$$

which characterizes the slip displacement required to transition from f_s to f_d, and which Rabinowicz found to be of the order of microns for metals.

More recent basic experiments on friction by Svetlizky & Fineberg [9] have confirmed by direct observation that frictional slip travels at relatively slow fronts leading behind regions of stick where the shear tractions show a square-root singularity typical of fracture mechanics. The strength of this singularity (which would be a material toughness in the case of the rupture of a bulk solid) is approximately constant, although it may depend on the local pressure. Indeed, motivated by Fineberg's observation, Ciavarella [10] extended classical solutions of contact problems where a tangential load is applied in the transition from static to sliding contact, to the case of a mode II stress-intensity factor around the stick-slip boundary. Further, Papangelo et al. [11] showed that this corresponds to the limit where the transition to kinetic slip occurs over a sufficiently small part of the contact area, and is analogous to the 'JKR' approximation for normal adhesion problems. In

this limit, a slip-dependent friction coefficient $f(u)$ can be approximated by a mode II stress-intensity factor

$$K = \sqrt{2E^* \left(f_s - f_d\right) p\Delta} \,, \tag{3}$$

where p is the local pressure and E^* is the composite elastic modulus defined by

$$\frac{1}{E^*} = \frac{(1-\nu_1^2)}{E_1} + \frac{(1-\nu_2^2)}{E_2} \,, \tag{4}$$

where $E_i, \nu_i,\ i = 1, 2$ are respectively Young's modulus and Poisson's ratio for the two materials. Using this approach, the solution of classical frictional contact problems can be extended to include the effect of slip-dependent friction. In this paper, we consider the implications for the problem of tractive rolling of a wheel.

2. The rolling contact problem

We consider the case of a cylindrical wheel of radius R rolling at speed V over a half plane and seek a solution that is invariant in the moving frame of reference $\xi = x - Vt$. If Dundurs' bimaterial constant $\beta = 0$, the solution depends on the elastic properties only through the composite elastic modulus of equation (4), so for simplicity, we can assume that the wheel is rigid and the half-plane is elastic. The contact pressure distribution is then given by

$$p(\xi) = p_0\sqrt{1 - \frac{\xi^2}{a^2}} \quad \text{where } p_0 = \frac{2P}{\pi a} \,; \quad a = 2\sqrt{\frac{PR}{\pi E^*}} \,, \tag{5}$$

a is the contact semi-width, and P is the normal contact force per unit thickness.

The stick [no slip] condition can be expressed as $\dot{u}_x(x,t) = \dot{U}$, where U is a relative rigid-body displacement. Thus, in the moving frame of reference,

$$-V\frac{du_x}{d\xi} = \dot{U} \,, \tag{6}$$

where $\dot{U}$ is the creep velocity.

Following Carter, we assume a stick zone $c < \xi < a$ adjacent to the leading edge, and we write the shear tractions $q(\xi)$ as the superposition of the full slip solution and a corrective term — i.e.

$$q(\xi) = f_d p(\xi) + q^*(\xi) \,, \tag{7}$$

where f_d is the kinetic friction coefficient and $q^*(\xi)$ is non-zero only in $c < \xi < a$. The corresponding tangential displacement gradients are then given by

$$\frac{du_x}{d\xi} = -\frac{2}{\pi E^*}\left(\int_{-a}^{a} \frac{f_d p(s)ds}{\xi - s} + \int_{c}^{a} \frac{q^*(s)ds}{\xi - s}\right), \tag{8}$$

and using (5, 6) we obtain

$$\int_{c}^{a} \frac{q^*(s)ds}{\xi - s} = \frac{\pi E^* \dot{U}}{2V} - \frac{\pi f_d E^* \xi}{2R} \quad c < \xi < a\,, \tag{9}$$

which is a Cauchy singular integral equation for $q^*(\xi)$.

We seek a solution that is bounded at the leading edge $\xi = a$, but singular with stress-intensity factor

$$K = \lim_{\xi \to c^+} q(\xi)\sqrt{2\pi(\xi - c)} \tag{10}$$

at the boundary $\xi = c$, where stick is transitioning to slip. The appropriate solution is

$$q^*(\xi) = f_d p_0 \sqrt{\left(1 - \frac{\xi}{a}\right)\left(\frac{\xi}{a} - \frac{c}{a}\right)} + \frac{K}{\sqrt{2\pi(a-c)}}\sqrt{\frac{a-\xi}{\xi - c}}\,, \tag{11}$$

for $c < \xi < a$. In the classical Carter solution, the shear traction is assumed to be less than $f_d p(\xi)$ throughout the stick zone, and this condition is satisfied only if $K = 0$, leaving just the first bounded-bounded term in equation (11). Figure 1 compares the Carter solution [dashed] with a representative Griffith friction solution (red line), for a given $c/a = -0.5$.

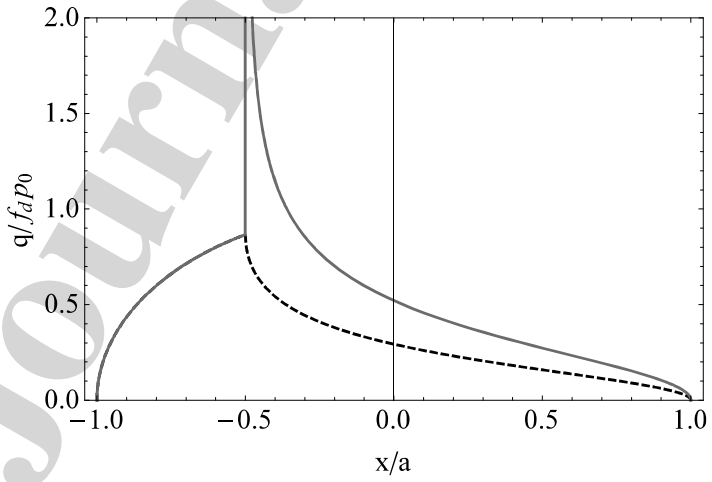

Fig.1: The shear tractions $q(\xi)$ from Eqs. (7, 11) for $c/a = -0.5$ and $\widehat{K}_{\max} = 0$ (dashed, original Carter solution), or $\widehat{K}_{\max} = 0.3$ (red line), where $\widehat{K}_{\max}$ is defined in equation (17).

For given values of c and K, the total tangential load Q can be obtained from (7, 11) as

$$\frac{Q}{f_d P} = 1 - \left(\frac{1 - c/a}{2}\right)^2 + \widehat{K}\sqrt{1 - c/a} \tag{12}$$

where we have defined

$$\widehat{K} = \frac{K\sqrt{\pi a}}{2\sqrt{2} f_d P} = \frac{K}{f_d p_0 \sqrt{2\pi a}} \tag{13}$$

The creep velocity $\dot{U}$ and hence the creep ratio $\zeta = \frac{\dot{U}}{V}$ can be found by substituting (11) into (9) and evaluating the integrals, with the result

$$\frac{\zeta}{\zeta_0} = \left[\left(\frac{1 + c/a}{2}\right) + \frac{\widehat{K}}{\sqrt{1 - c/a}}\right] \tag{14}$$

where

$$\zeta_0 = \frac{f_d a}{R} \tag{15}$$

We also record the corresponding expression for the shear tractions (7) which is

$$\frac{q(\xi)}{f_d p_0} = \sqrt{1 - \left(\frac{\xi}{a}\right)^2} - \sqrt{\left(1 - \frac{\xi}{a}\right)\left(\frac{\xi}{a} - \frac{c}{a}\right)} + \frac{\widehat{K}}{\sqrt{1 - c/a)}}\sqrt{\frac{a - \xi}{\xi - c}}\,, \tag{16}$$

where the square roots are to be interpreted as zero in ranges where their arguments are negative.

2.1. Slip-weakening law

Equation (3) shows that the stress-intensity factor K depends on the local pressure p at the stick-slip boundary, which is here given by (5) with $\xi = c$. Using these results in (13), we obtain

$$\widehat{K} = \widehat{K}_{\max}\left(1 - \left(\frac{c}{a}\right)^2\right)^{1/4} \text{ where } \widehat{K}_{\max} = \sqrt{\frac{E^*\left(f_s - f_d\right)\Delta}{\pi f_d^2 a p_0}} \tag{17}$$

and hence

$$\frac{Q}{f_d P} = 1 - \frac{1}{4}\left(1 - \frac{c}{a}\right)^2 + \widehat{K}_{\max}\left(1 - \frac{c}{a}\right)^{3/4}\left(1 + \frac{c}{a}\right)^{1/4}, \tag{18}$$

$$\frac{\zeta}{\zeta_0} = \frac{1}{2}\left(1 + c/a\right) + \widehat{K}_{\max}\left(\frac{a+c}{a-c}\right)^{1/4}, \tag{19}$$

from (12, 14).

3. Results

Fig.2 shows the traction ratio $Q/f_d P$ as a function of c/a from Eq. (18), where as before, the original Carter solution ($\widehat{K}_{\max} = 0$) is represented by a black dashed line, and the red line represents the case $\widehat{K}_{\max} = 0.3$. Notice that the singular solution defines two possible states corresponding to the same traction ratio in the range $Q/f_d P > 1$. We shall argue below that the dashed part of this curve, where $Q/f_d P$ is a decaying function of c/a, is unstable under load control.

The corresponding creep ratio ζ/ζ_0 is shown as a function of c/a in Fig. 3. Notice that the creep ratio increases without limit as $c \to a$ in contrast to the original Carter solution which exhibits a transition from microslip to sliding at a finite creep rate ζ_0.

Finally, in Fig. 4, we use c/a as a parameter in Eqs. (18, 19) to generate a parametric plot of the traction ratio as a function of creep ratio. If the system is operating under load control, and if the velocity is given an infinitesimal perturbation when operating in the dashed [negative slope] region, it is clear that the resulting change in Q will cause the system to accelerate away from the equilibrium state, indicating instability. Depending on the sign of the perturbation, the system would either revert to the stable solution in the rising portion of the curve, or the creep rate would increase without limit. The dashed portion of the curve is however meaningful if the creep rate is prescribed — i.e. if the velocities or the two rollers are prescribed kinematically.

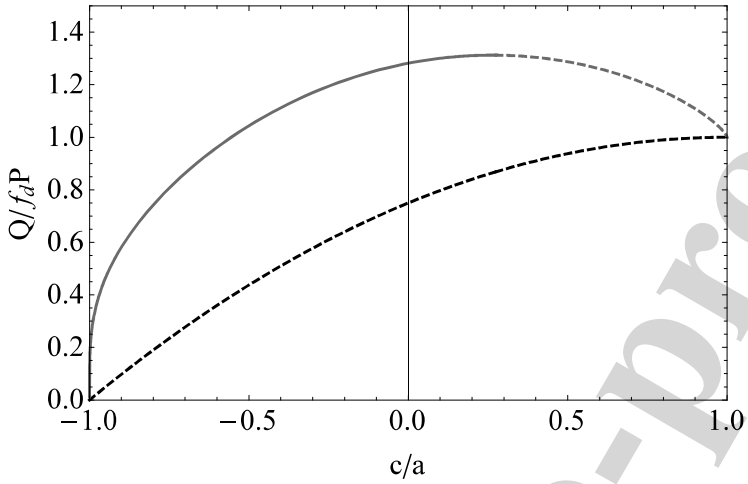

Fig.2: The traction ratio Q/f_dP as a function of the ratio stick area to contact area (c/a) from Eq. (18). The dashed black line represents Carter's original solution ($\widehat{K}_{\max} = 0$), and the red line represents $\widehat{K}_{\max} = 0.3$, where $\widehat{K}_{\max}$ is defined in equation (17).

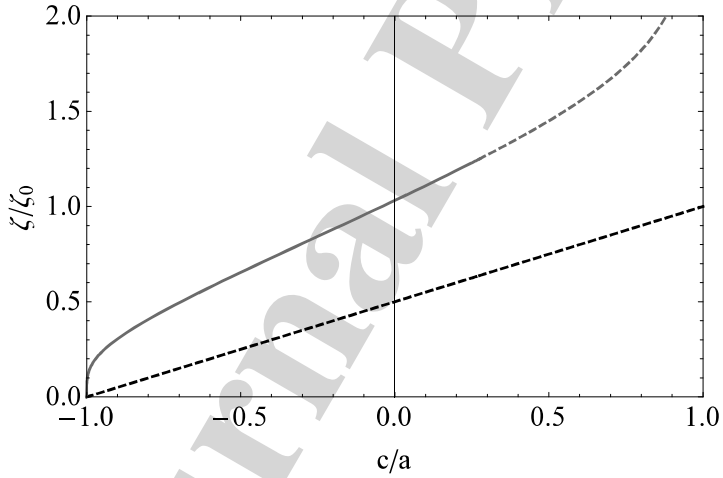

Fig.3: The creep ratio ζ/ζ_0 as a function of the ratio stick area to contact area (c/a) from Eq. (19). The dashed black line represents Carter's original solution ($\widehat{K}_{\max} = 0$), and the red line represents $\widehat{K}_{\max} = 0.3$, where $\widehat{K}_{\max}$ is defined in equation (17).

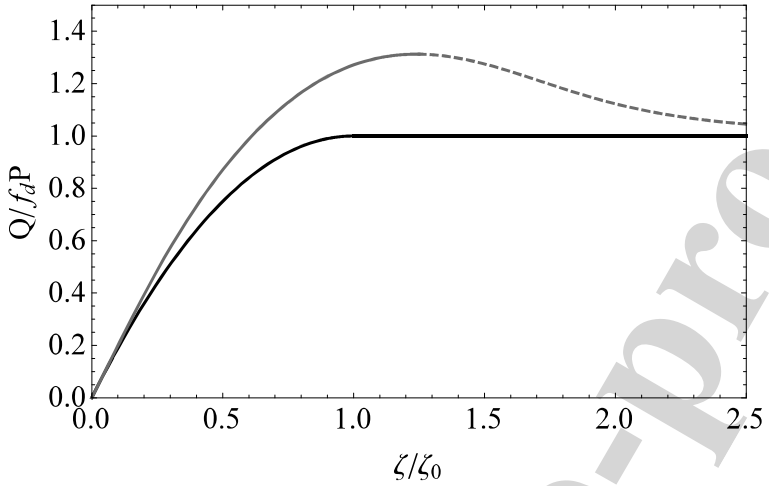

Fig.4: Parametric plot of the traction ratio Q/f_dP as a function of creep ratio ζ/ζ_0 from Eqs. (18,19). The black line represents Carter's original solution ($\widehat{K}_{\max} = 0$), and the red line represents $\widehat{K}_{\max} = 0.3$, where $\widehat{K}_{\max}$ is defined in equation (17). Points on the dashed red line are unstable under load control.

4. Extension to 3D rolling with Kalker's strip theory

Kalker [2] (see also [12], par.18.3.5) used Carter's solution as the basis of an approximate solution for the rolling of bodies with quadratic surfaces for cases where the Hertzian contact ellipse is elongated in the y-direction perpendicular to the rolling direction, x. Applications include the rolling of a ball in an almost conforming groove, or the rolling of slightly misaligned cylinders. Conditions then vary relatively slowly in the y-direction and it is reasonable to approximate the tractions as locally two-dimensional.

Kalker's solution is easily extended to the case of Griffith friction using the results of Section 2. The contact pressure is

$$p(\xi,\eta) = p_0\sqrt{1-\xi^2-\eta^2} \quad \text{where} \quad \xi = \frac{x}{a}\ ;\ \ \eta = \frac{y}{b}\ ;\ \ p_0 = \frac{3P}{2\pi ab}\ , \tag{20}$$

a, b are the contact semi-axes with $b \gg a$, and P is the normal force.

The half-width of the contact area and the local peak contact pressure at location η are then given by

$$a_1(\eta) = a\sqrt{1-\eta^2}\ ;\quad p_1(\eta) = p_0\sqrt{1-\eta^2}\ , \tag{21}$$

and the local value of the dimensionless stress-intensity factor $\widehat{K}_{\max}$ is

$$\widehat{K}^1_{\max}(\eta) = \sqrt{\frac{E^*(f_s - f_d)\Delta}{\pi f_d^2 a_1(\eta) p_1(\eta)}} = \frac{\widehat{K}_{\max}}{\sqrt{1-\eta^2}} \,, \tag{22}$$

where $\widehat{K}_{\max}$ is defined in Eq. (17).

The local creep rate is then given by Eq. (19) with $a_1(\eta), c_1(\eta), \widehat{K}^1_{\max}(\eta), p_1(\eta)$ replacing $a, c, \widehat{K}_{\max}, p_0$. We obtain

$$\frac{\zeta}{\zeta_0} = \frac{1}{2}\left(\frac{a_1(\eta)+c_1(\eta)}{a}\right) + \widehat{K}_{\max}\left(\frac{a_1(\eta)+c_1(\eta)}{a_1(\eta)-c_1(\eta)}\right)^{1/4} \,, \tag{23}$$

where ζ_0 is redefined as $2f_d p_0/E^*$, with p_0 being defined in (20). Kinematic considerations show that ζ must be independent of η, so this equation implicitly defines the function $c_1(\eta)$ for given ζ.

Notice that in the original Carter solution $\widehat{K}_{\max} = 0$, so $a_1 + c_1$ is constant showing that the stick-slip boundary is simply a reflection of part of the leading edge of the contact. By contrast, when $\widehat{K}_{\max} > 0$, the stick zone extends throughout the leading edge to $y = \pm b$, though it may be asymptotically small near the ends.

Eq. (18) defines the tangential force per unit length in the y-direction if $a, c, \widehat{K}_{\max}$ are replaced by $a_1(\eta), c_1(\eta), \widehat{K}^1_{\max}(\eta)$ and P is replaced by the integral of the pressure across the strip which is $\pi a_1 p_1/2$. The total tangential force can then be obtained by integration. After some algebra, we obtain

$$\frac{Q}{f_d P} = \frac{3}{4}\int_{-1}^{1}\left[\frac{a_1^2}{a^2} - \left(\frac{a_1 - c_1}{2a}\right)^2 + \widehat{K}_{\max}\left(\frac{a_1}{a} - \frac{c_1}{a}\right)^{3/4}\left(\frac{a_1}{a} + \frac{c_1}{a}\right)^{1/4}\right] d\eta \,, \tag{24}$$

where P is now the total normal force in the 3D problem. Notice that Eqs. (23, 24) do not contain b and hence the solution is independent of the eccentricity of the ellipse, provided this is sufficiently large to justify the initial approximation.

Figure 5 shows the relationship between the traction ratio $Q/f_d P$ and the creep ratio ζ/ζ_0. 3D solutions are shown as solid lines and the corresponding 2D solutions as dashed lines. The Carter solutions are shown in black, and the singular solutions [with $\widehat{K}_{\max} = 0.3$] in blue. The 3D solution is very close to the 2D solution for the non-singular Carter case in the entire range

of validity, but the corresponding singular solutions are close only for low creep ratios. The maximum traction ratio achievable is significantly lower for the 3D solution – a result of the fact that the stress-intensity factor decreases towards the edges together with the peak pressure.

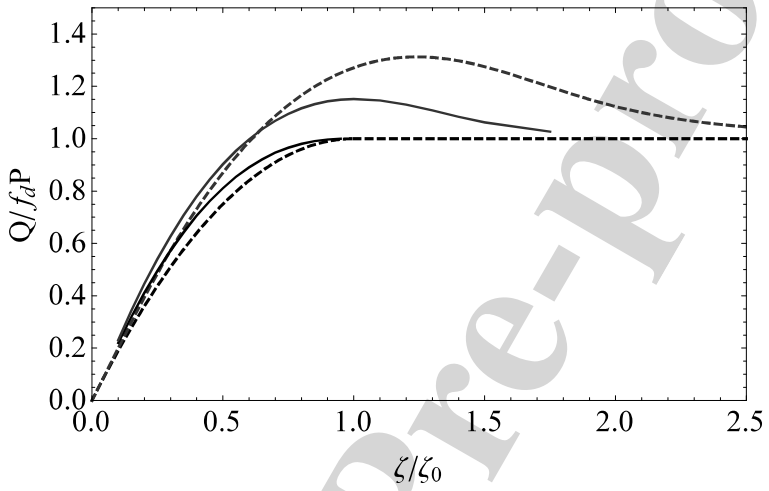

Fig.5: Traction ratio Q/f_dP as a function of creep ratio ζ/ζ_0 from Eqs. (23, 24). The black line represents Carter's original solution ($\widehat{K}_{\max} = 0$), and the blue line represents $\widehat{K}_{\max} = 0.3$, where $\widehat{K}_{\max}$ is defined in equation (17). The corresponding two-dimensional results from Fig. 4 are shown as dashed lines for comparison. Notice that Q and P represent load per unit thickness in the 2D solutions.

5. Discussion

In contrast to the original Carter solution, we predict that there is a creepage-weakening range, which is qualitatively supported by experimental evidence.

Figure 6 shows a comparison between the proposed model with the Griffith singularity factor described by Eqs. (17)-(19), Carter's solution, and measured data in Ref.[13]. The data were collected from a railway wheel (with typical geometrical parameters $R = 500$ and $a \approx 5$ mm) with an axle load of 22.5 tons subjected to pure longitudinal creepage. The model parameters for plotting the figure were adjusted to match the initial slope of

the creepage-force law, assuming secondary effects connected to the presence of roughness and interfacial layers of contaminants require this modification, as commonly done also by other authors [3]. One drawback of our solution is that for different wheel speed V, the curve remains the same, contrary to experimental evidence.

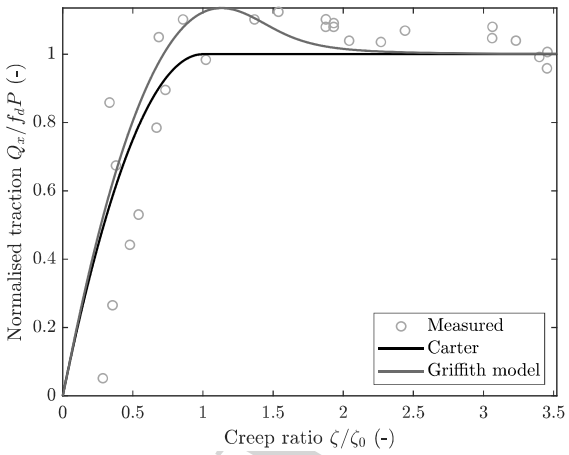

Fig.6: Traction ratio Q/f_dP as a function of creep ratio ζ/ζ_0 in Carter's original solution, present solution (parameter values: $\hat{K}_{\max} = 0.3$, $f_d = 0.21$ and $\zeta_0 = 0.015$), and experimental data [13].

Indeed, Vollebregt [3] in an attempt to fit experimental data for longitudinal creepage for the Siemens locomotive Eurosprinter 127001 for pure longitudinal creepage, finds two sources of disagreement over the classical Carter solution. One is the falling friction regime, which continues to occur also for very large creep ratios, much beyond the expected saturation (full slip), for which he postulates a *slip rate dependent* friction law, which then is implemented numerically not without difficulties associated to some instabilities — and this effect was in the present paper appropriately taken into account. Secondly, a much reduced slope in the "elastic" initial traction vs creepage law is found, which he attributes to layers of third body materials at the interface between the rail and the wheel (contaminants, debris, or maybe roughness itself). The slope reduction in practice depends linearly on the layer flexibility, and geometry, but since the constitutive equations and thickness of the layers are difficult to estimate, the slope reduction is mostly a fit to experiments.

While we cannot rule out that slip-rate friction law terms are also at play, we have provided an alternative explanation of the falling curve due to elastic deformation for the low creepage regime. In trying to fit experimental results reported in [3] for the tractive coefficient Q/P as a function of longitudinal creepage for pure longitudinal creepage, our solution gives rise to an even greater initial slope for the traction ratio vs creepage curve than the original Carter's one, and the indication of Ref.[3] of the need to consider an interfacial layer of contaminants needs a fortiori to be considered.

6. Conclusion

We have given a simple extension of the celebrated Carter solution with a friction law which passes abruptly from a static to a dynamic friction coefficient. In contrast to the original Carter solution, we predict that there is a creepage-weakening range, which is qualitatively supported by experimental evidence. The effect of the change in friction can be significant, as from our estimates, also on the global level of resulting forces and creepage. We estimate a 3D solution using Kalker's strip theory, showing that the effect of the singular shear tractions is reduced due to the edges being at lower pressures.

Acknowledgements

MC acknowledges support from the Italian Ministry of Education, University and Research (MIUR) under the program "Departments of Excellence" (L.232/2016).

7. References

[1] Carter, F. W. (1926). On the action of a locomotive driving wheel. Proceedings of the Royal Society of London. Series A, containing papers of a mathematical and physical character, 112(760), 151-157.

[2] Kalker, J. J. (2013). Three-dimensional elastic bodies in rolling contact (Vol. 2). Springer Science & Business Media.

[3] Vollebregt, E. A. H. (2014). Numerical modeling of measured railway creep versus creep-force curves with CONTACT. Wear, 314(1-2), 87-95.

[4] Fletcher, D. I., & Lewis, S. (2013). Creep curve measurement to support wear and adhesion modelling, using a continuously variable creep twin disc machine. Wear, 298, 57-65.

[5] Polach, O. (2005). Creep forces in simulations of traction vehicles running on adhesion limit. Wear, 258(7-8), 992-1000.

[6] Ding, B., Squicciarini, G., Thompson, D., & Corradi, R. (2018). An assessment of mode-coupling and falling-friction mechanisms in railway curve squeal through a simplified approach. Journal of Sound and Vibration, 423, 126-140.

[7] Xie, G., Allen, P. D., Iwnicki, S. D., Alonso, A., Thompson, D. J., Jones, C. J., & Huang, Z. Y. (2006). Introduction of falling friction coefficients into curving calculations for studying curve squeal noise. Vehicle system dynamics, 44(sup1), 261-271.

[8] Rabinowicz E. 1951The nature of the static and kinetic coefficients of friction. J. Appl. Phys. 22, 1373–1379.

[9] Svetlizky I, Fineberg J. 2014Classical shear cracks drive the onset of dry frictional motion. Nature 509, 205–208.

[10] Ciavarella, M. (2015). Transition from stick to slip in Hertzian contact with "Griffith" friction: The Cattaneo–Mindlin problem revisited. Journal of the Mechanics and Physics of Solids, 84, 313-324.

[11] Papangelo, A., Ciavarella, M., & Barber, J. R. (2015). Fracture mechanics implications for apparent static friction coefficient in contact problems involving slip-weakening laws. Proceedings of the Royal Society A: Mathematical, Physical and Engineering Sciences, 471(2180), 20150271.

[12] Barber, J. R. (2018). Contact mechanics (Vol. 250). Springer.

[13] Six, K. , Meierhofer, A., Müller, G., Dietmaier, P. (2015). Physical processes in wheel-rail contact and its implications on vehicle-track interaction, Vehicle System Dynamics: International Journal of Vehicle Mechanics and Mobility, Vol. 53:5, 635-650.

Carter's problem of a wheel under tractive rolling is extended to slip-dependent friction.

A fracture mechanics solution is found the shear tractions, which describes some aspects of "falling friction" creepage forces

In experiments probably friction includes also rate-dependent effects.

3D effects reduce the strength of the singularity at the edges being the peak pressure lower there.

Declaration of interests

☒ The authors declare that they have no known competing financial interests or personal relationships that could have appeared to influence the work reported in this paper.

☐ The authors declare the following financial interests/personal relationships which may be considered as potential competing interests: